

BRIEF COMMUNICATION

[¹⁸F]AV-1451 binding is increased in frontotemporal dementia due to C9orf72 expansion

Richard W. Bevan-Jones¹, Thomas E. Cope², Simon P. Jones², Luca Passamonti², Young T. Hong³, Tim Fryer³, Robert Arnold¹, Jonathan P. Coles⁴, Franklin A. Aigbirhio³, Karalyn Patterson^{2,5}, John T. O'Brien^{1,*} & James B. Rowe^{2,5,*}

¹Department of Psychiatry, University of Cambridge, Cambridge, United Kingdom

²Department of Clinical Neurosciences, University of Cambridge, Cambridge, United Kingdom

³Wolfson Brain Imaging Centre, University of Cambridge, Cambridge, United Kingdom

⁴Division of Anaesthesia, University of Cambridge, Cambridge, United Kingdom

⁵Medical Research Council Cognition and Brain Sciences Unit, Cambridge, United Kingdom

Correspondence

Richard W. Bevan-Jones, Herchel Smith Building, Cambridge Biomedical Campus, Hills Road, Cambridge CB2 0SZ. Tel: 01223 760699; Fax: 01223 760696; E-mail: wrb22@medschl.cam.ac.uk

Funding Information

The work was supported by National Institute for Health Cambridge Research Biomedical Research Centre; the Wellcome Trust (JBR 103838); the Association of British Neurologists and the Patrick Berthoud Charitable Trust (TEC).

Received: 3 April 2018; Revised: 7 June 2018; Accepted: 20 July 2018

Annals of Clinical and Translational Neurology 2018; 5(10): 1292–1296

doi: 10.1002/acn3.631

*Joint Senior authors.

Introduction

[¹⁸F]AV-1451 was developed as a specific marker of paired helical filament tau (PHF-tau) pathology in Alzheimer's disease (AD), and is selective for PHF-tau over beta-amyloid and alpha-synuclein *in vitro*.¹ *In vivo* studies have confirmed elevated and distributed binding in keeping with typical and atypical presentations of Alzheimer's disease,^{2,3} consistent with Braak staging.⁴ Binding characteristics in neurodegenerative diseases other than Alzheimer's disease are controversial.

In vivo and *post mortem* studies indicate increased [¹⁸F]AV-1451 binding in patients with frontotemporal dementia due to mutations in the microtubule-associated

Abstract

The PET ligand [¹⁸F]AV-1451 was developed to bind tau pathology in Alzheimer's disease, but increased binding has been shown in both genetic tauopathies and in semantic dementia, a disease strongly associated with TDP-43 pathology. Here we assessed [¹⁸F]AV-1451 binding in behavioral variant frontotemporal dementia due to a hexanucleotide repeat expansion in C9orf72, characterized by TDP-43 pathology. We show that the C9orf72 mutation increases binding in frontotemporal cortex, with a distinctive distribution of binding compared with healthy controls.

protein tau (MAPT), albeit with differences between mutations associated with paired helical filament tauopathy and straight filament tauopathy.^{5,6} Regionally elevated binding also occurs in another tauopathy, progressive supranuclear palsy.^{7,8} However, [¹⁸F]AV-1451 binding is also seen in patients with semantic dementia, a disease strongly associated with TAR DNA-binding Protein-43 (TDP-43), especially type C.^{9,10} The non-tau target of [¹⁸F]AV-1451 binding in semantic dementia is unknown and, whilst *post mortem* studies suggest a lack of binding to TDP-43 pathology,^{11–13} the elevated binding seen *in vivo* is in keeping with the characteristic anatomical distribution of neuropathology in semantic dementia.

A limitation of previous studies of $[^{18}\text{F}]\text{AV-1451}$ binding in semantic dementia cases is their reliance on clinico-pathological correlations to interpret the neuroimaging data. In this report, we describe $[^{18}\text{F}]\text{AV-1451}$ binding in a patient with a clear familial case of frontotemporal dementia (FTD) due to a hexanucleotide repeat expansion in the C9orf72 gene. This is the commonest genetic cause of FTD¹⁴ and it is strongly associated with TDP-43 pathology¹⁵ without the presence of any tau. We examine not only the magnitude of the $[^{18}\text{F}]\text{AV-1451}$ binding, but also the pattern of regional distribution across cortical and subcortical structures.

Case and Controls

A 53-year-old man presented with a 3-year history of progressive behavioral change characterized by disinhibition, grandiosity, and stereotyped behaviors. He subsequently developed semantic impairments and anomia, with loss of single word comprehension and surface dyslexia. At the time of imaging, he scored 53/100 on the Addenbrooke's Cognitive Examination – revised edition (ACE-R, reference range >88) and 25/30 on the Mini Mental State Examination (MMSE). There were significant carer endorsements for changes in memory, challenging behaviors, altered eating habits and abnormal beliefs on the revised Cambridge Behavioural Inventory. Structural magnetic resonance imaging of his brain confirmed frontotemporal atrophy. His maternal uncle had died of motor neurone disease. Genetic testing confirmed a hexanucleotide repeat expansion in C9orf72. He met diagnostic criteria for definite behavioral variant frontotemporal dementia.^{16,17} He underwent research structural MRI and $[^{18}\text{F}]\text{AV-1451}$ positron emission tomography (PET) as part of the Neuroimaging of Inflammation in Memory and Related Other Disorders (NIMROD) study.¹⁸ Thirteen healthy volunteers acted as controls (age range 55–80, 6 Male, ACE-R range 89–99, MMSE range 28–30) and underwent the same neuroimaging and behavioral protocol.

Data Modeling and Statistical Method

When comparing the case with the C9orf72 genetic expansion and controls, two questions were posed. First, were there regions of the brain with increased nondisplaceable-binding potential (BP_{ND})? Secondly, irrespective of the absolute level of ligand binding, did the distribution of binding across brain regions differ? This second question focusses on the multivariate distribution or pattern of binding, in relation to the distribution of neuropathological substrates of frontotemporal dementias.

The pattern may be abnormal, even where no single region on its own has particularly high binding of $[^{18}\text{F}]\text{AV-1451}$.

To address the first question, the brain was parcellated into 83 regions, using the Hammersmith atlas n30r83 modified to include some additional subcortical structures.⁷ The $[^{18}\text{F}]\text{AV-1451}$ BP_{ND} in each region was calculated using the methods described in Passamonti *et al.*⁷ to obtain regional BP_{ND} which were adjusted for cerebrospinal fluid (CSF) partial volume effects. Individual *t*-tests were then performed in each region to compare the observed $[^{18}\text{F}]\text{AV-1451}$ BP_{ND} in the C9orf72 case and controls, correcting for multiple comparisons across the full data range (FDR correction, $P < 0.05$, plus illustration at the more liberal threshold of $P < 0.05$ uncorrected).

To address the second question, a hierarchical cluster analysis was used. The CSF corrected and parcellated $[^{18}\text{F}]\text{AV-1451}$ BP_{ND} data were then converted to individual linear vectors containing all regions of interest. The pairwise Spearman's rank order correlations were calculated between all subjects, and the inverse taken to produce a dissimilarity matrix. This represents the difference in $[^{18}\text{F}]\text{AV-1451}$ BP_{ND} distribution between every pair of subjects, blinded to the absolute level of that binding. These dissimilarity measures were used to calculate a linkage dendrogram using an average distance method.

We also compared regional gray matter volume between the case and control group. Regional gray matter volumes were calculated during PET processing and parcellated, using the same atlas. For each region, linear models were used with region volume, age and total intracranial volume as covariates.¹⁹ *T*-tests were performed between the residual of the patient's volume and predicted volume, based on the controls' regression, and the control residuals. The *P*-values for each test were increased to compensate for the degrees of freedom used in the control regression. False discovery rate (FDR) correction was then applied to these adjusted *P*-values in the same manner as the $[^{18}\text{F}]\text{AV-1451}$ BP_{ND} .

Results

$[^{18}\text{F}]\text{AV-1451}$ in C9orf72 FTD versus controls

T1-weighted MPRAGE images are shown in Figure 1A and raw BP_{ND} images uncorrected for partial volume effects in Figure 1B. The left frontotemporal regions demonstrated increased BP_{ND} in the C9orf72 case compared to controls. After correcting for multiple comparisons ($P < 0.05$ FDR), significant abnormalities were observed in left fusiform gyrus, left medial anterior temporal lobe, left middle and inferior temporal gyri, and left

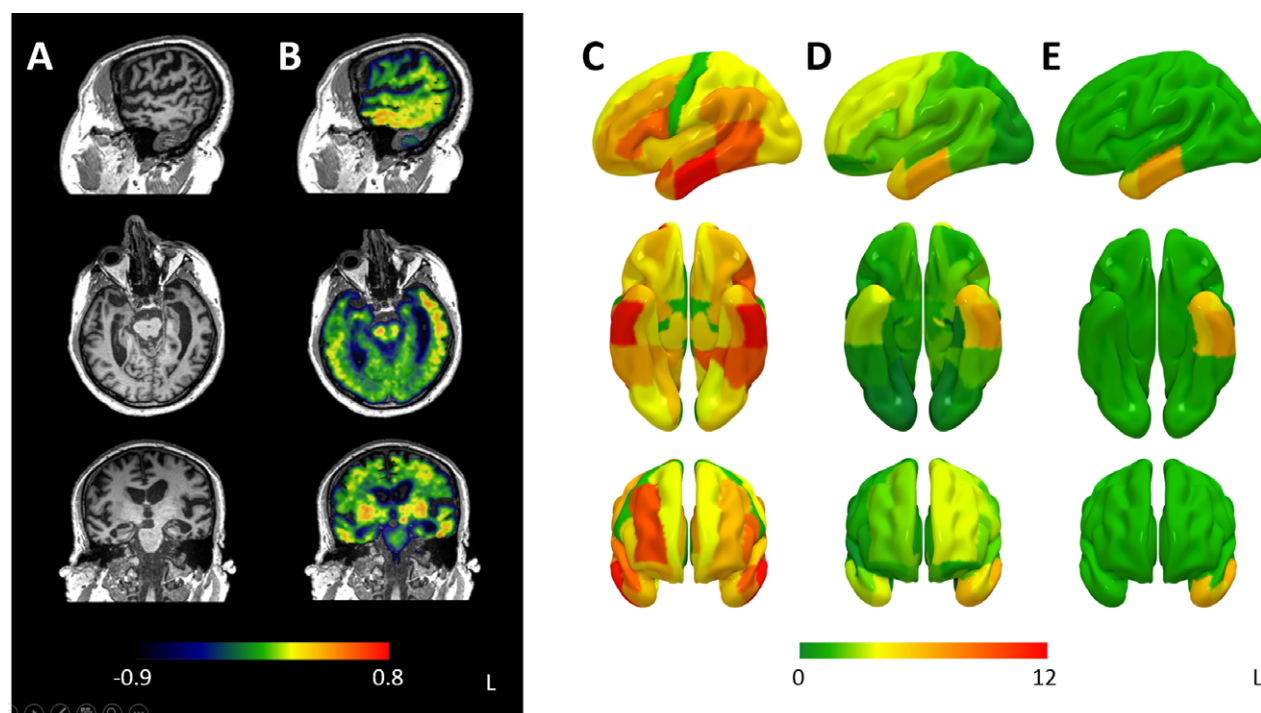


Figure 1. Panel A shows selected sagittal, coronal and axial slices from the structural MRI (T1-weighted MPRAGE) of the C9orf72 case. Panel B shows the [¹⁸F]AV-1451-binding potential (BP_{ND}) without correction for partial volume effects in the same planes. Panel C shows the unthresholded t-scores for gray matter atrophy on a volumetric rendering on the smoothed MNI152 template MRI. Panel D shows unthresholded t-scores for (BP_{ND}) in the same way. Panel E shows the same data but thresholded at $p < 0.05$ corrected for false discovery rate.

lateral inferior temporal lobe (Fig. 1E). In addition to this, more liberal thresholding without correction for multiple comparisons demonstrated bilateral changes, with elevated BP_{ND} also found in the right medial anterior temporal lobe, left anterior superior temporal gyrus, superior and middle frontal gyri, pallidum, and substantia nigra (Fig. 1D).

The distribution of BP_{ND} was also clearly dissimilar in the C9orf72 case compared to all controls (Figure S1A). The hierarchical clustering analysis indeed classified the patient as an outlier compared to controls (Figure S1B).

The regional volume analysis revealed widespread gray matter loss, most marked in the temporal lobes, which remained after FDR correction (Fig. 1C). *T*-scores along with FDR corrected *P*-values for both [¹⁸F]AV-1451 and gray matter volume are shown in Table S1.

Discussion

C9orf72 expansions are strongly associated with TDP-43 type B and dipeptide repeat pathology. We therefore infer that at 53 years old, with the C9orf72 expansion, and a classical FTD presentation, the present case has TDP-43 pathology without tauopathy. Despite this, the participant exhibited elevated [¹⁸F]

AV-1451 binding in frontotemporal regions of a magnitude greater than the 95th centile of binding in controls but within the interquartile range for binding in Alzheimer's disease⁷ and semantic dementia⁹ (Fig. 2). Combined with similar findings in 14 cases with semantic dementia,^{9,10} this suggests that the [¹⁸F]AV-1451 PET ligand is not specific for tau over TDP-43 pathology in Frontotemporal lobar degeneration. Therefore, while [¹⁸F]AV-1451 might retain a role in tracking disease by visualising the distribution and/or severity of neuropathology in a person with frontotemporal dementia, it is unlikely to have utility for cohort selection for disease modifying trials that target tau or TDP-43-specific disease mechanisms.

As expected in this participant with moderate dementia from a C9orf72 expansion, there was widespread gray matter loss with a predilection for frontotemporal regions, and particularly temporal regions in keeping with his clinical syndrome. The regions of elevated BP_{ND} with largest t-scores were situated within the atrophic regions but elevated BP_{ND} did not occur across all atrophic regions. The collocation of elevated BP_{ND} and atrophy is perhaps unsurprising if [¹⁸F]AV-1451 is binding to a non-tau molecule associated with C9orf72-related neurodegeneration.

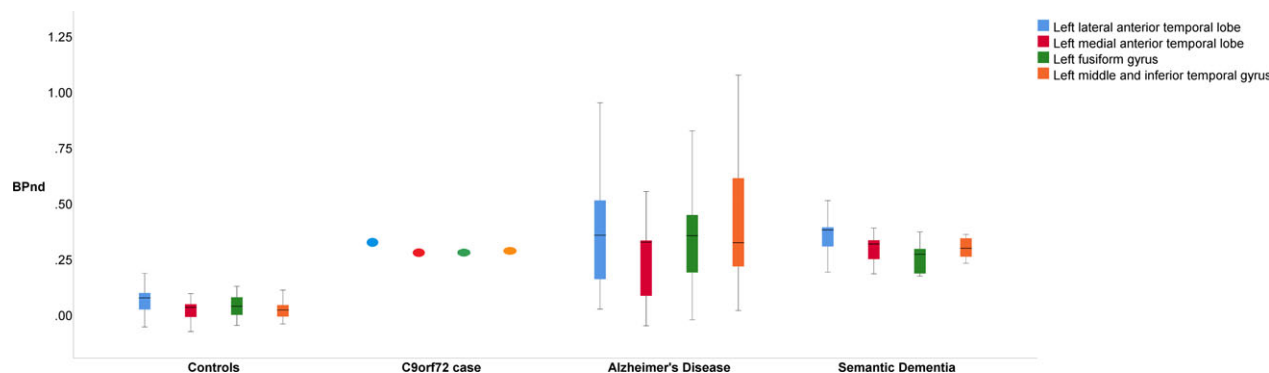


Figure 2. Boxplots of the nondisplaceable $[^{18}\text{F}]\text{AV-1451}$ -binding potential in those regions of interest that are significantly elevated in the C9orf72 case compared to controls after FDR correction. As well as data for the C9orf72 case and the control population, comparative data are shown using the same analysis methods for our previously published cohorts with Alzheimer's disease⁷ and Semantic Dementia⁹.

There are limitations in this study. First we have analysed data from a single case against a control group. Larger studies in C9orf72 FTD might expand upon these results, as C9orf72 frontotemporal dementia is clinically and neuroanatomically heterogeneous.²⁰ While our C9orf72 case is young, mutation positive, and meets diagnostic criteria for definite behavioral variant frontotemporal dementia, we lack biomarker or pathology proof of the absence of coincidental Alzheimer tau pathology that may occur in a small percentage of adults in their fifties. However, age-related presymptomatic Alzheimer pathology is rendered an unlikely explanation for our data, both by the low population prevalence at 53, and the regions found to have elevated binding in our case which are clearly distinct from those usually observed in Alzheimer's disease. Finally, we note that the calculation of $[^{18}\text{F}]\text{AV-1451}$ BP_{ND} data uses the superior cerebellar gray matter as a reference region, as in our other recent papers.^{5,7,9} Although across most of the genetic and sporadic forms of FTD this region remains unaffected, in previous cases with C9orf72 expansion, cerebellar atrophy and dipeptide aggregation have been described.²¹ In mitigation of this potential shortcoming, whilst as expected there was cerebellar gray matter atrophy in the present C9orf72, there was no observable elevated cerebellar $[^{18}\text{F}]\text{AV-1451}$ signal in the uncorrected PET BP_{ND} map. Moreover, if elevated binding in this reference cerebellar region were present, it would have only reduced the estimated BP_{ND} elsewhere, making the risk of false negative results more likely. In any case, it is important to note that the level of cerebellar binding does not affect the non-parametric analysis of distributional-binding differences.

Elevated binding in genetic TDP-43-associated FTD provides further evidence for anatomically specific binding of $[^{18}\text{F}]\text{AV-1451}$ to non-tau targets. However, the sensitivity to longitudinal changes in TDP-43-associated FTD, and the molecular identity of the $[^{18}\text{F}]\text{AV-1451}$ target, remain to be determined.

Author Contributions

WRBJ wrote the first draft, all other authors provided review and critique of manuscript. JBR, JTOB, FIA, TDF and KP conceptualized and designed the study. WRBJ, TDF, YTH and JPC were integral to the organization and execution of the study. WRBJ, TEC and PSJ designed and executed the statistical analysis, KP, LP and JBR provided statistical review and critique.

Acknowledgments

We thank the staff at the Wolfson Brain Imaging Centre and Addenbrooke's Hospital and the NIHR Dementias and Neurodegenerative Diseases Research Network. We thank Dr's Istvan Boros and Joong-Hyun Chun for manufacture of $[^{18}\text{F}]\text{AV-1451}$ and Avid (Lilly) for supplying the ligand precursor. The work was supported by National Institute for Health Cambridge Research Biomedical Research Centre; the Wellcome Trust (JBR 103838); the Association of British Neurologists and the Patrick Berthoud Charitable Trust (TEC).

Conflict of Interest

JOB has acted as a consultant for GE Healthcare and Lilly.

References

- Xia C, Arteaga J, Chen G, et al. $[^{18}\text{F}]$ T807, a novel tau positron emission tomography imaging agent for Alzheimer's disease. *Alzheimer's Dement* 2013;9:666–676.
- Ossenkoppele R, Schonhaut DR, Schöll M, et al. Tau PET patterns mirror clinical and neuroanatomical variability in Alzheimer's disease. *Brain* 2016;139:1551–1567. Accessed at: <http://brain.oxfordjournals.org/%5Cnhttp://www.ncbi.nlm.nih.gov/pubmed/26962052>.

3. Scholl M, Ossenkoppele R, Strandberg O, et al. Distinct 18 F-AV-1451 tau PET retention patterns in early- and late-onset Alzheimer's disease. *Brain* 2017;140:1–9.
4. Schwarz AJ, Yu P, Miller BB, et al. Regional profiles of the candidate tau PET ligand 18 F-AV-1451 recapitulate key features of Braak histopathological stages. *Brain* 2016;139:1539–1550. Accessed at: <http://www.brain.oxfordjournals.org/lookup/doi/10.1093/brain/aww023>.
5. Bevan-Jones WR, Cope TE, Passamonti L, et al. [¹⁸F]AV-1451 PET in behavioral variant frontotemporal dementia due to MAPT mutation. *Ann Clin Transl Neurol* 2016;3:940–947. Accessed at: <https://doi.org/doi.wiley.com/10.1002/acn3.366>.
6. Smith R, Ohlsson T, Puschmann A, et al. F-AV-1451 tau PET imaging correlates strongly with tau neuropathology in MAPT mutation carriers. *Brain* 2016;139:1–8.
7. Passamonti L, Vazquez Rodriguez P, Hong YT, et al. 18F-AV-1451 positron emission tomography in Alzheimer's disease and progressive supranuclear palsy F-AV-1451 positron emission tomography in Alzheimer's disease and progressive supranuclear palsy. *Brain* 2017;140:1–11.
8. Cope TE, Rittman T, Borchert RJ, et al. Tau burden and the functional connectome in Alzheimer's disease and progressive supranuclear palsy. *Brain J Neurol* 2018;141:550–567.
9. Bevan-Jones WR, Cope TE, Jones PS, et al. [¹⁸F] AV-1451 binding in vivo mirrors the expected distribution of TDP-43 pathology in the semantic variant of primary progressive aphasia. *J Neurol Neurosurg Psychiatry* 2017;88:1–6.
10. Makarets SJ, Quimby M, Collins J, et al. Flortaucipir tau PET imaging in semantic variant primary progressive aphasia. *J Neurol Neurosurg Psychiatry* 2017;88:1–8.
11. Marquié M, Normandin MD, Vanderburg CR, et al. Validating novel tau positron emission tomography tracer [¹⁸F]-AV-1451 (T807) on postmortem brain tissue. *Ann Neurol* 2015;78:787–800.
12. Sander K, Lashley T, Gami P, et al. Characterization of tau positron emission tomography tracer [¹⁸F]AV-1451 binding to postmortem tissue in Alzheimer's disease, primary tauopathies, and other dementias. *Alzheimer's Dement* 2016;12:1116–1124.
13. Lowe VJ, Curran G, Fang P, et al. An autoradiographic evaluation of AV-1451 Tau PET in dementia. *Acta Neuropathol Commun* 2016;4:58. Accessed at: <http://actaneurocomms.biomedcentral.com/articles/10.1186/s40478-016-0315-6>.
14. Bang J, Spina S, Miller BL. Frontotemporal dementia. *Lancet* 2015;386:1672–1682. Elsevier Ltd. Accessed at: [https://doi.org/10.1016/s0140-6736\(15\)00461-4](https://doi.org/10.1016/s0140-6736(15)00461-4).
15. Mackenzie IRA, Neumann M, Baborie A, et al. A harmonized classification system for FTLD-TDP pathology. *Acta Neuropathol* 2011;122:111–113.
16. Rascovsky K, Hodges JR, Knopman D, et al. Sensitivity of revised diagnostic criteria for the behavioural variant of frontotemporal dementia. *Brain* 2011;134:2456–2477.
17. Gorno-Tempini ML, Hillis AE, Weintraub S, et al. Classification of primary progressive aphasia and its variants. *Neurology* 2011;76:1006–1014.
18. Bevan-Jones WR, Surendranathan A, Passamonti L, et al. Neuroimaging of Inflammation in Memory and Related Other Disorders (NIMROD) study protocol: a deep phenotyping cohort study of the role of brain inflammation in dementia, depression and other neurological illnesses. *BMJ Open* 2017;7:1–9.
19. O'Brien LM, Ziegler DA, Deutsch CK, et al. Statistical adjustments for brain size in volumetric studies: some practical implications in methods. *Psychiatry Res* 2012;193:113–122.
20. Devenney E, Hornberger M, Irish M, et al. Frontotemporal dementia associated with the C9ORF72 mutation. *JAMA Neurol* 2014;71:331. Accessed at: <http://archneur.jamaneurology.com/article.aspx?doi=10.1001/jamaneurol.2013.6002>.
21. Mackenzie IR, Arzberger T, Kremmer E, et al. Dipeptide repeat protein pathology in C9ORF72 mutation cases: clinico - pathological correlations. *Acta Neuropathol* 2013;126:859–879.

Supporting Information

Additional supporting information may be found online in the Supporting Information section at the end of the article.

Figure S1. (A) Spearman dissimilarity matrix (1-correlation) between all individuals. The first row and column, separated by black lines from the other rows and columns, represents the patient. The other thirteen columns represent controls. (B) the average linkage dendrogram produced by hierarchical cluster analysis. The two resultant clusters are colored in red and black.

Table S1. Displaying T-scores and FDR corrected p-values for [¹⁸F]AV-1451-binding potential and for atrophy in each region, ordered by magnitude of [¹⁸F]AV-1451-binding potential T-score.